JACS
JOURNAL OF THE AMERICAN CHEMICAL SOCIETY
Article
pubs.acs.org/JACS

Supramolecular Copolymers: Structure and Composition Revealed by Theoretical Modeling

Anindita Das,[†,‡,⊥] Ghislaine Vantomme,[†,‡,⊥] Albert J. Markvoort,[‡,§] Huub M. M. ten Eikelder,[*,‡,§] Miguel Garcia-Iglesias,[†,‡] Anja R. A. Palmans,[*,†,‡] and E. W. Meijer[*,†,‡]

[†]Laboratory of Macromolecular and Organic Chemistry, Eindhoven University of Technology, P.O. Box 513, 5600 MB Eindhoven, The Netherlands

[‡]Institute for Complex Molecular Systems, Eindhoven University of Technology, P.O. Box 513, 5600 MB Eindhoven, The Netherlands

[§]Computational Biology Group, Eindhoven University of Technology, P.O. Box 513, 5600 MB Eindhoven, The Netherlands

Supporting Information

ABSTRACT: Supramolecular copolymers, non-covalent analogues of synthetic copolymers, constitute a new and promising class of polymers. In contrast to their covalent counterparts, the details of their mechanism of formation, as well as the factors determining their composition and length, are still poorly understood. Here, the supramolecular copolymerization between two slightly structurally different benzene-1,3,5-tricarboxamide (BTA) monomers functionalized with either oligodimethylsiloxane (oDMSi) or alkyl side chains is unraveled by combining experimental and theoretical approaches. By applying the "sergeant-and-soldiers" approach using circular dichroism (CD) experiments, we are able to obtain detailed insights into the structure and composition of these supramolecular copolymers. Moreover, we observe an unexpected chiral induction upon mixing two independently CD-silent solutions of the achiral (soldier) and chiral (sergeant) monomers. We find that the subtle differences in the chemical structure of the two monomers impact their homopolymerization mechanism: whereas alkyl-BTAs cooperatively self-assemble, oDMSi-BTAs self-assemble in an isodesmic manner. The effect of these mechanistic differences in the supramolecular copolymerization process is investigated as a function of the composition of the two monomers and explicitly rationalized by mathematical modeling. The results show that, at low fractions of oDMSi-BTA sergeants (<10 mol%), the polymerization process is cooperative and the supramolecular helicity is biased toward the helical preference of the sergeant. However, at higher fractions of oDMSi-BTA sergeant (>25 mol%), the isodesmic assembly of the increasing amounts of sergeant becomes more dominant, and different species start to coexist in the copolymerization process. The analysis of the experimental data with a newly developed theoretical model allows us to quantify the thermodynamic parameters, the distribution of different species, and the compositions and stack lengths of the formed supramolecular copolymers existing at various feed ratios of the two monomers.

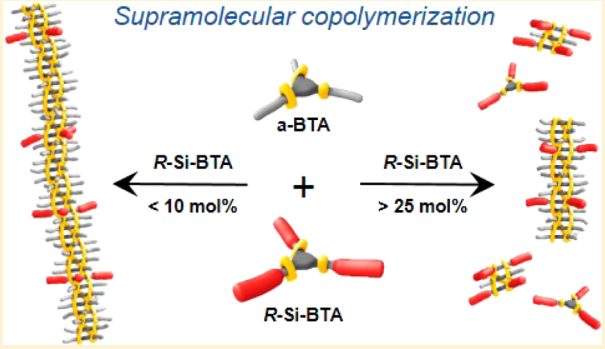

INTRODUCTION

Copolymerizing different monomers offers vast possibilities to tune the properties of covalent copolymers. In fact, the ability to copolymerize monomers in an alternating, gradient, random, or block manner offers superb precision in the control over the copolymer's molecular structure (composition, sequence, and length).[1] As a result, a wide range of material properties can be readily accessed. Generally, the molecular structure of the copolymer can be predicted and tuned by a delicate interplay of reactivity and feed ratios of the two monomers via the classical copolymer equation,[2] in combination with advanced controlled polymerization techniques.[3]

In the field of supramolecular copolymers,[4] in contrast, much less attention has been devoted to developing predictive rules that allow to forecast the sequence, composition, and length of multicomponent mixtures. The dynamic nature of the non-covalent interactions makes multifunctional supramolecular copolymers versatile systems, which gives them a high potential for use as adaptive materials,[5] in organic electronics,[6] and as biomimetic systems.[7] However, constructing hierarchical multi-component co-assemblies is particularly challenging as it requires a rational design that encompasses a subtle balance between the complementary recognizing motifs for connecting different monomers into an ordered array and the compatibility between the diverse peripheral functional groups. Moreover, important differences are encountered when copolymers made under thermodynamic equilibrium are compared with those

Received: March 22, 2017
Published: May 9, 2017

DOI: 10.1021/jacs.7b02835
J. Am. Chem. Soc. 2017, 139, 7036−7044

Scheme 1. Chemical Structures of Benzene-1,3,5-tricarboxamides

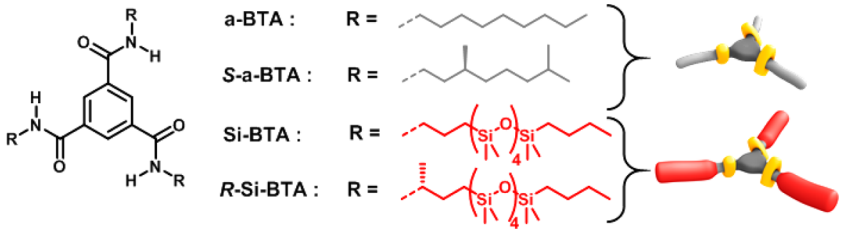

Table 1. Thermodynamic Parameters for the Self-Assembly of Solutions of a-BTA into a 1/1 Mixture of *P*/*M*-Type Aggregates and *R*-Si-BTA into *X*-Type Aggregates in MCH, Determined by Fitting the Temperature-Dependent Spectroscopy Data into a One-Component Model

compound	ΔH^0_e (kJ·mol^{-1})	ΔS^0_e (kJ·mol^{-1}·K^{-1})	ΔH^0_n (kJ·mol^{-1})	σ
a-BTA	−65	−0.104	−45	3.1×10^{-4}
***R*-Si-BTA**	−35	−0.044	−35	1

prepared under kinetic control. When mixing different types of monomers, two extreme assembly cases may occur; total self-sorting or complete co-assembly of the different monomers. Many elegant examples have been presented in which multicomponent co-assembly has been achieved by aromatic donor−acceptor interactions,[8] hydrogen bonding,[9] π-stacking interactions,[10] and others.[11] In addition, multicomponent systems are also found to form self-sorted assemblies.[12] A comprehensive molecular understanding on which of these cases will dominate is often less studied.[12c,g,h]

Recently, significant progress has been made in the elucidation of pathway complexity, mechanistic detail, feed-dependent behavior, thermodynamic stability, composition, and stack length of supramolecular (co)polymerizations.[13−15] Exciting examples are found in kinetically controlled living copolymerizations as developed for covalent block copolymers[11e−h] and small molecules,[13c−g] which show that kinetically trapped block structures can be formed in supramolecular copolymers. For systems under thermodynamic equilibrium, a combined experimental and theoretical approach proved to be a robust method to unravel several issues, although these endeavors were typically limited to one-component or simple two-component systems.[14d,e,15a,b] However, in many examples reported on multicomponent systems, these characteristics remain largely elusive, particularly when the components aggregate via different supramolecular polymerization mechanisms.

In the past, our group has extensively studied the helical, one-dimensional self-assembly of chiral and achiral alkyl-substituted BTAs (**alkyl-BTAs**),[16] which follows a highly cooperative mechanism in dilute aliphatic solvents.[17] The handedness of the helical superstructures, *P* or *M*, is biased by the presence of a non-racemic stereocenter in the aliphatic side chains. In contrast, the self-assembly of BTAs functionalized with short oligodimethylsiloxane (oDMSi) chains (**oDMSi-BTA**) revealed a decrease in propensity for assembly compared to alkyl-substituted BTAs, which was attributed to the presence of sterically crowded siloxanes.[18] The presence of oDMSi side chains in BTA-derivatives increased the critical aggregation concentration 10−100 times over that of **alkyl-BTAs**, but the mechanism of self-assembly remained unclear. In addition, we also observed that unsymmetrical BTAs comprising both oDMSi and alkyl side chains form a superlattice in the bulk due to strong phase separation of the two chemically incompatible side chains.[18]

An intriguing question is how BTAs with either oDMSi or alkyl side chains would interact in solution. In a mixture of **alkyl-BTA** and **oDMSi-BTA**, three outcomes are possible: (1) alternate copolymerization to minimize steric demand of **oDMSi-BTAs**; (2) complete self-sorting due to peripheral chain incompatibility; or (3) everything in between. To elucidate these possibilities, we herein perform "sergeant-and-soldiers" experiments[19] between opposite pairs of chiral and achiral **alkyl-BTA** and **oDMSi-BTA** derivatives (Scheme 1). A combination of chiral (optically active) and achiral BTAs permits the observation of copolymerization behavior by circular dichroism (CD) spectroscopy. An unexpected chiral induction was observed from the mixture of two independently CD-silent solutions of achiral **alkyl-BTA** (**a-BTA**) and chiral **oDMSi-BTA** (***R*-Si-BTA**). A detailed analysis was conducted to understand how the differences in molecular structure and polymerization pathway of individual monomers affect the chiral amplification and the overall copolymerization process by combining spectroscopic studies with in-depth theoretical modeling. In the present work, we propose a general experimental/modeling approach to understand various aspects of supramolecular copolymerization under thermodynamic control. This collective approach permits us to successfully elucidate the monomer feed-dependent copolymerization behavior and thereby the composition of the supramolecular copolymers obtained. In the present report, before studying the copolymerization between **alkyl-BTA** and **oDMSi-BTA**, we first revisit the mechanism of homopolymerization of the individual components. The copolymerization is then analyzed by the mixing of the two monomers in different ratios. Finally, we put forward a new theoretical model that permits to fully explain the copolymerization process.

RESULTS

Supramolecular Homopolymerization of alkyl-BTA and oDMSi-BTA. Before studying the copolymerization behavior, we first analyzed the mechanism of homopolymerization of the individual monomers. The self-assembly of chiral ***R*-Si-BTA** in methylcyclohexane (MCH) was probed using temperature- and concentration-dependent CD measurements and compared to that of achiral **a-BTA** under identical conditions. The synthesis of both compounds was reported previously.[17a,18] The experimental cooling curves were fitted with a one-component mass-balance model (Figures S1 and

DOI: 10.1021/jacs.7b02835
J. Am. Chem. Soc. 2017, 139, 7036−7044

S2).[14a,d] This model is based on the equilibrium between monomers, oligomers, and polymers, and the aggregation process is divided into a nucleation regime and an elongation regime. The equilibrium constant K_n describes the formation of a nucleus, whereas K_e describes the equilibrium constant in the elongation phase. The nucleation step is highly unfavorable in a cooperative process so that $K_n < K_e$. In an isodesmic process, K_n and K_e are equal. The degree of cooperativity in the supramolecular polymerization is given by the cooperativity factor σ defined as K_n/K_e. Increasingly small numbers for σ indicate an increase in cooperativity of the system. The thermodynamic parameters obtained for **a-BTA** and ***R*-Si-BTA** are summarized in Table 1 and detailed in the Supporting Information. The ΔH^0_e of −35 kJ/mol for ***R*-Si-BTA** in combination with σ = 1 indicates that the assembly is enthalpically driven and occurs via an isodesmic mechanism. Interestingly, at lower concentration (10 μM in MCH), the UV−vis spectrum (Figure S3) shows aggregation but the solution of ***R*-Si-BTA** is CD silent (Figure 1B). This suggests

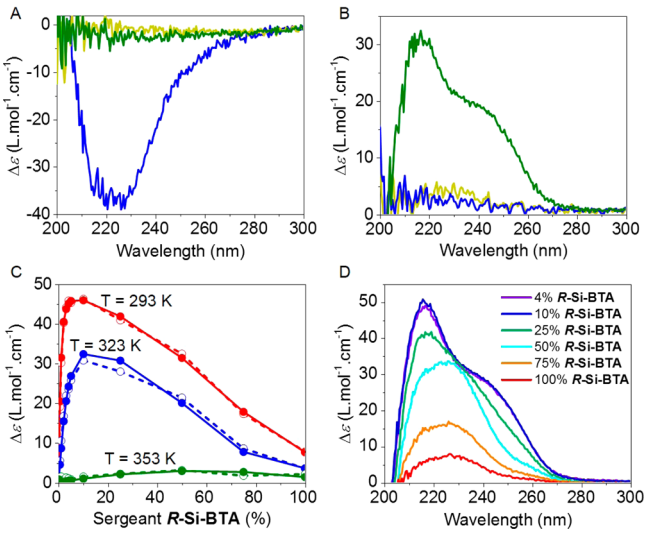

Figure 1. (A) CD spectra of ***S*-a-BTA** (blue trace), **Si-BTA** (yellow trace), and the mixture (green trace) of ***S*-a-BTA** (4 mol%) + **Si-BTA** (96 mol%) at c_{tot} = 10 μM in MCH at 298 K. (B) CD spectra of ***R*-Si-BTA** (blue trace), **a-BTA** (yellow trace), and the mixture (green trace) of ***R*-Si-BTA** (4 mol%) + **a-BTA** (96 mol%) at c_{tot} = 10 μM in MCH at 298 K, showing chiral amplification from two individually CD-silent solutions. (C) Experimental and calculated (vide infra) $\Delta\varepsilon$ (determined from the CD effect at 220 nm) as a function of the percentage of sergeant ***R*-Si-BTA** added to the soldier **a-BTA** at c_{tot} = 50 μM at three different temperatures. Experimental data are represented by a dashed line and calculated values by a solid line. (D) CD spectra of various mixtures of **a-BTA** and ***R*-Si-BTA** at c_{tot} = 50 μM at 293 K.

the formation of (disordered) dimers or short aggregates (referred to as *X*-type aggregates) which comprise a different conformation of the hydrogen bonds that hardly contributes to the CD signal. As inferred from the one-component model and expected for an isodesmic mechanism, the *X*-type aggregates predominantly consist of dimers at this low concentration (Figure S4). In contrast, under identical conditions (10 μM in MCH) **a-BTA** cooperatively self-assembles into equal amounts of right-handed (*P*) and left-handed (*M*) helical aggregates of significantly longer length (average stack length of over 200 monomers per stack at 298 K), with thermodynamic parameters consistent with those previously found for similar BTAs.[20] These aggregates are known to be stabilized by ordered, three-fold helical hydrogen bonding.[16]

More insight into the differences of the hydrogen bonding patterns between the two BTAs was inferred from infrared (IR) spectroscopy measurements. The comparison of the IR spectra of 1.0 mM MCH solutions of **a-BTA** and ***R*-Si-BTA** shows different C═O vibration bands of the homopolymers suggesting differences in the hydrogen bonding patterns within the aggregates formed by **a-BTA** and ***R*-Si-BTA** (Figure S5). The introduction of the three sterically demanding oDMSi groups at the periphery of the BTA core not only destabilizes the self-assembly as elucidated from its lower enthalpy of elongation ΔH^0_e (−35 kJ·mol^{-1}) compared to **a-BTA** (−65 kJ·mol^{-1}) but also alters the nature of the hydrogen bonds within the aggregates.

Supramolecular Copolymerization of alkyl- and oDMSi-BTAs. In our previous work,[17a,18] we performed "sergeant-and-soldiers" experiments[19] on scalemic mixtures of ***S*-Si-BTA/Si-BTA** and ***S*-a-BTA/a-BTA**. In both cases, a complete helical sense bias was achieved at 10 mol% for ***S*-Si-BTA** and only 4 mol% for ***S*-a-BTA**. We continued with investigating the supramolecular copolymerization between **alkyl-BTA** and **oDMSi-BTA** of opposite pairs of chiral ***S*-a-BTA** and achiral **Si-BTA**, and of chiral ***R*-Si-BTA** and achiral **a-BTA**, respectively (Scheme 1, Figure 1A, B). All the four monomers feature an identical three-fold self-complementary amide array that can recognize either monomers of identical or different side chains for homopolymerization or copolymerization, respectively. The molar circular dichroism values ($\Delta\varepsilon$) of the individual solutions and the mixtures were measured at a total BTA concentration of 10 μM in MCH.

Strikingly, we here find that a mixture of 4 mol% of chiral ***S*-a-BTA** mixed with the 96 mol% of achiral soldiers **Si-BTA** is CD silent (Figure 1A), although ***S*-a-BTA** on its own shows a large CD signal ($\Delta\varepsilon$ = −38 L·mol^{-1}·cm^{-1}). This could be due to three possibilities: (1) the chiral sergeant ***S*-a-BTA** fails to bias the helicity of the achiral **Si-BTA** soldiers due to immiscibility between ***S*-a-BTA** and **Si-BTA**, resulting from side chains' incompatibility;[18] (2) the fraction of ***S*-a-BTA** is too small (4 mol%) to bias the helicity of the **Si-BTA** stacks; or (3) **Si-BTA** fails to form long aggregates at the applied concentration (9.6 μM). This third possibility is supported by the theoretical one-component model which shows that, at the applied concentration of 10 μM, **Si-BTA** predominantly exists as dimers in MCH (Figure S4).

Contrastingly, in the opposite set of experiments where ***R*-Si-BTA** plays the role of sergeant, 4 mol% of the chiral sergeant ***R*-Si-BTA** did successfully bias the helical preference of a large excess (96 mol%) of achiral **a-BTA** soldiers. Figure 1B shows appearance of a large CD signal within the mixture, indicative of strong chiral amplification, while the two homopolymer solutions were CD-silent. Such observation is not unique[9b] but still remarkable in the sense that the strong CD effect arises from the mixing of two CD-silent dilute solutions, underlining a strong interaction between the two monomers. Combining the two sets of experiments, we conclude that **oDMSi-BTA** is a "good sergeant" for the **alkyl-BTA** soldiers (Figure 1B) whereas a "bad soldier" for **alkyl-BTA** sergeants (Figure 1A). Therefore, unlike previously reported sergeants, we present herein a BTA that effectively biases the helical sense preference of achiral alkyl-based BTAs, but is incapable to efficiently function as a soldier. This observation is in line with those for

DOI: 10.1021/jacs.7b02835
J. Am. Chem. Soc. 2017, 139, 7036−7044

crowded amino-acid-based BTAs recently disclosed by us and Bouteiller and co-workers, which were also excellent sergeants for achiral alkyl BTAs.[21]

To investigate the copolymerization in more detail, we gradually increased the fraction of the ***R*-Si-BTA** sergeant in a mixture with **a-BTA** soldiers, keeping the total monomer concentration constant at 50 μM, and monitored the changes in the molar circular dichroism ($\Delta\varepsilon$) at 220 nm at three different temperatures. A nonlinear variation of $\Delta\varepsilon$ was observed, and two distinct regimes were distinguished (Figure 1C). In the first regime, a strong nonlinear increase in the molar circular dichroism was observed with the addition of ***R*-Si-BTA** sergeant. At 293 K, a maximum was reached at 4 mol%, which coincides with the fraction of sergeant reported earlier for "sergeant-and-soldiers" experiments with aliphatic alkyl-BTAs.[17a] However, above 10 mol% of ***R*-Si-BTA**, a continuous decrease of the molar circular dichroism was observed, reaching a minimum at 100 mol% ***R*-Si-BTA**. This observation indicates that at higher fraction of bulky ***R*-Si-BTA** another process is taking over that either decreases the helical sense bias or affects the nature of the formed supramolecular aggregates. This observation is also in sharp contrast to "sergeant-and-soldiers" experiments earlier performed between either chiral and achiral **alkyl-BTAs** or **oDMSi-BTAs**, that revealed near saturation in the CD-signal above 10 mol% of the alkyl sergeant.[17a,18]

In order to elucidate the origin of this intriguing behavior of ***R*-Si-BTA** in the mixed aggregates, we closely inspected the full CD spectra of all the mixtures with increasing fraction of ***R*-Si-BTA**. Two distinctly different patterns in the shape of the CD spectra can be discerned (Figure 1D): at low fractions of sergeant, up to ~10 mol%, the CD spectrum shows a double Cotton effect with a maximum at 220 nm and a shoulder at ~245 nm, but at higher fractions of sergeant (>25 mol%), the CD spectrum changes to the spectrum of pure sergeant, with a single maximum at 225 nm. Such differences in the CD spectra of the mixtures can be attributed to a different packing of the hydrogen bonds within the helical stacks below 10 mol% and above 25 mol% ***R*-Si-BTA**.[14e,17e] The difference in molecular packing was also evident from the FT-IR data of 1 mM MCH solutions of 10 mol% and 90 mol% of *R*-Si-BTA that showed resemblance with pure **a-BTA** and ***R*-Si-BTA**, respectively (Figure S5).

To further elucidate this change in the shape of the CD signal as a function of increasing fraction of ***R*-Si-BTA**, variable-temperature UV and CD experiments were carried out at various compositions of ***R*-Si-BTA/a-BTA** in MCH at a total BTA concentration of 50 μM (Figures 2 and 3). Interestingly, two different trends in the UV and CD cooling curves are observed. Up to 5 mol% of ***R*-Si-BTA** sergeant added, all the UV cooling curves are superimposable to the curve of pure **a-BTA**, indicating a similar cooperative mechanism of copolymerization as observed for **a-BTA** homopolymer (Figure 2A). However, above the threshold of 5 mol% of ***R*-Si-BTA**, the melting curves gradually become more sigmoidal (Figures 2B and 3B), indicating a change toward an isodesmic growth mechanism.

To rationalize these observations, we hypothesize that the two monomers can copolymerize into aggregates in which the monomer present in majority dictates the molecular packing/aggregate properties. At lower fractions of ***R*-Si-BTA**, **a-BTA** dominated cooperative helical aggregates are formed contributing to the huge CD signal whereas at higher fractions of ***R*-Si-BTA**, ***R*-Si-BTA** dominated isodesmic aggregates (*X*-type) are

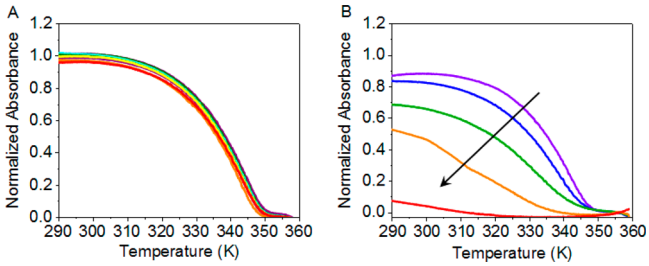

Figure 2. Temperature-dependent UV spectra of solutions containing different ratios of ***R*-Si-BTA/a-BTA** probed at λ = 220 nm with c_{tot} = 50 μM in MCH (cooling rate = 2 K·min^{-1}). (A) Going from violet curve (0 mol% ***R*-Si-BTA**) to red curve (5 mol% ***R*-Si-BTA**), upon addition of 1 mol%, 2 mol%, 3 mol%, and 4 mol% of ***R*-Si-BTA** to **a-BTA**. (B) Going from violet curve (10 mol% ***R*-Si-BTA**) to red curve (100 mol% ***R*-Si-BTA**), upon addition of 25 mol%, 50 mol%, and 75 mol% of ***R*-Si-BTA** to **a-BTA**.

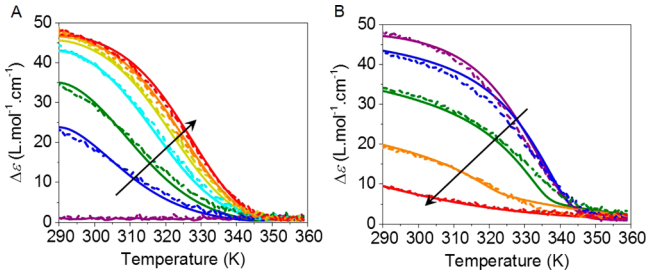

Figure 3. Experimental and computed (vide infra) CD cooling curves probed at λ = 220 nm with c_{tot} = 50 μM in MCH containing different ratios of ***R*-Si-BTA/a-BTA** (cooling rate = 2 K·min^{-1}). (A) Going from violet curve (0 mol% ***R*-Si-BTA**) to red curve (5 mol% ***R*-Si-BTA**), upon addition of 0.5 mol%, 1 mol%, 2 mol%, 3 mol%, and 4 mol% of ***R*-Si-BTA** to **a-BTA**. (B) Going from violet curve (10 mol% ***R*-Si-BTA**) to red curve (100 mol% ***R*-Si-BTA**), upon addition of 25 mol%, 50 mol%, and 75 mol% of ***R*-Si-BTA** to **a-BTA**. Experimental data are represented by dashed lines, while computed values are represented by solid lines.

assembled but participate with low CD intensity. As the current experimental techniques available do not allow defining the precise nature of the assemblies at such low concentration, we resort to theoretical models to understand the copolymerization in more detail.

Theoretical Model for Two-Component Copolymerization. A model describing two-component copolymerization was put forward to explain the origin of the remarkable chiral amplification followed by steep fall in the CD signal observed in the "sergeant-and-soldiers" experiments performed between independently CD-silent solutions of **a-BTA** (named A in the model) and ***R*-Si-BTA** (named Si in the model). This new model is an extension of the one-component model, but now with two monomers and three types of aggregates, namely *P*, *M*, and *X*. The current model takes into account not only distinct dimers and elongation steps but also the types of bonds formed between different monomers in the stacks. The reaction scheme is described as a sequence of stepwise monomer associations and dissociations, where the equilibrium constants are assumed to depend not only on the aggregate type but also on the types of the two monomers involved in the bond formed/broken, and whether it concerns the nucleation of a new aggregate or the elongation of an existing one (see Supporting Information section B for details). The equilibrium concentrations of all species are obtained by solving the mass-

DOI: 10.1021/jacs.7b02835
J. Am. Chem. Soc. 2017, 139, 7036−7044

balance equations for the two monomers, and these are subsequently used to calculate theoretical CD and/or UV absorption cooling curves. This methodology has been applied previously to describe both the "majority-rules" and the "sergeant-and-soldiers" principles in cooperative two-component BTA supramolecular polymerization.[14d,15a,b] Herein, we assume that ***R*-Si-BTA** forms enantiomeric isodesmic *X*-type aggregates (with thermodynamic parameters as reported in Table 1) while the **a-BTA** forms racemic cooperative aggregates with two opposite helicities, i.e., *P*- and *M*-type aggregates, with equal likelihood (again with thermodynamic parameters as reported in Table 1, $\Delta G^0_{\text{A-PM}}$). Moreover, we assume that **a-BTA** can mix into *X*-type aggregates ($\Delta G^0_{\text{A-X}}$) and, vice versa, that ***R*-Si-BTA** can mix into both *P*- ($\Delta G^0_{\text{Si-P}}$) and *M*-type ($\Delta G^0_{\text{Si-M}}$) aggregates, by forming **a-BTA**/***R*-Si-BTA** bonds. Additionally, we consider that the formation of ***R*-Si-BTA**/***R*-Si-BTA** bonds within cooperative *P*- and *M*-type aggregates and **a-BTA**/**a-BTA** bonds in isodesmic *X*-type aggregates are energetically unfavorable, therefore they are not considered in the model. An optimal fit of the theoretical CD curves (Figure 3, solid lines) with the experimental CD curves (Figure 3, dashed lines) is obtained with the thermodynamic parameters shown in Table 2 (see Supporting Information section B for details). Figure 4 shows that the UV melting curves calculated by this newly developed two-component model also demonstrate nice agreement with the experimental curves (Figure 2). Note that these UV curves are results of the model, with parameters that were fitted only with CD curves, which further illustrates the potential of the model to describe the experimental data.

Table 2. Thermodynamic Parameters, ΔH^0 and ΔS^0, for the Co-assembly of a-BTA and *R*-Si-BTA in MCH, Determined by Fitting the Temperature-Dependent CD Data with the Two-Component Model

aggregate	ΔH^0 (kJ·mol^{-1})	ΔS^0 (kJ·mol^{-1}·K^{-1})
A–X	−48.4	−0.070
Si–P (n)[a]	−26.6	−0.057
Si–P (e)[b]	−46.6	−0.057
Si–M (n)[a]	−43.0	−0.115
Si–M (e)[b]	−63.0	−0.115

[a]"n" refers to the nucleation step. [b]"e" refers to the elongation step.

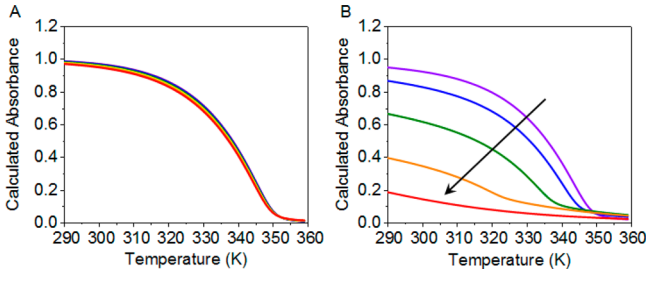

Figure 4. Calculated UV curves obtained from the model showing the theoretical normalized absorbance as a function of temperature. (A) Going from violet curve (0.5 mol% ***R*-Si-BTA**) to red curve (5 mol%), upon addition of 1 mol%, 2 mol%, 3 mol%, and 4 mol% of ***R*-Si-BTA** to **a-BTA**. (B) Going from violet curve (10 mol% ***R*-Si-BTA**) to red curve (100 mol% ***R*-Si-BTA**), upon addition of 25 mol%, 50 mol%, and 75 mol% of ***R*-Si-BTA** to **a-BTA**. These model results show a similar spectral trend as observed in the experimental UV cooling curves in Figure 2.

As is evident from the thermodynamic parameters of the copolymerization as a function of the temperature in Figure 5,

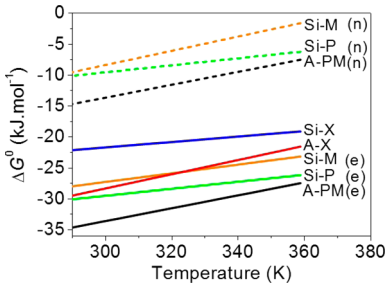

Figure 5. Temperature-dependent free energies ($\Delta G^0 = \Delta H^0 - T\Delta S^0$) of the co-assemblies compared with those of the homopolymers.

the mixing of ***R*-Si-BTA** into *M*- or *P*-type aggregates is less favorable than the addition of **a-BTA** ($\Delta G^0_{\text{A-PM}} < \Delta G^0_{\text{Si-P}}$ and $\Delta G^0_{\text{A-PM}} < \Delta G^0_{\text{Si-M}}$). However, because of the chirality of ***R*-Si-BTA**, this sergeant intercalates slightly better into *P*-type aggregates than into *M*-type aggregates ($\Delta G^0_{\text{Si-M}} > \Delta G^0_{\text{Si-P}}$). In addition, the incorporation of **a-BTA** and ***R*-Si-BTA** into *X*-type aggregates is less energetically favorable than their incorporation into cooperative *P*- or *M*-aggregates ($\Delta G^0_{\text{A-PM}} < \Delta G^0_{\text{A-X}}$ and $\Delta G^0_{\text{Si-P}} < \Delta G^0_{\text{Si-M}} < \Delta G^0_{\text{Si-X}}$).

Apart from quantifying the thermodynamic parameters, this model also reveals the distribution of different species present at each ***R*-Si-BTA** fraction as a function of temperature via speciation plots[22] (Figure 6). At lower fractions of the sergeants ***R*-Si-BTA**, the cooperative mechanism of **a-BTA** assembly (*P*- and *M*-type) dominates over the isodesmic assembly of the *X*-type aggregates, and a competition between *P*- and *M*-type stacks is observed (Figure 6A–C). Without sergeants, *P*- and *M*-type aggregates are equally abundant (Figure S6), while with increasing fractions of sergeants (>0.5 mol%), the *P*-type aggregates rapidly prevail over the *M*-type aggregates. The lower the temperature, the smaller the fraction of sergeant needed to solely have *P*-type aggregates. The largest quantity of *P*-type aggregates is obtained with a fraction of ***R*-Si-BTA** of around 10 mol%, which is in agreement with the experimental observations. Moreover, for higher fractions of sergeants (>25 mol%), the isodesmic *X*-type aggregates start to compete with the *P*-type aggregates (Figure 6D,E). When the quantity of ***R*-Si-BTA** is preponderant (>75 mol%), the isodesmic *X*-type aggregates prevail over the cooperative *P*-type aggregates (Figure 6F), and a dominant isodesmic mechanism is observed in the mixture resulting in a fall in the CD intensity. Figure 7A shows the calculated amounts of different species formed as a function of the addition of sergeants at 293 K and predicts the coexistence of *P*- and *M*-type aggregates above 10 mol% of sergeant added. For *P*-type aggregates, the number of monomers per aggregate decreases when the fraction of sergeants increases (Figure 7B).

To gain insight into the composition of the distinct aggregate types, the percentages (Figure S7) and concentrations (Figure S8) of sergeants ***R*-Si-BTA** constituting the *P*- and *X*-type aggregates over sergeants added were plotted, clearly indicating that the compositions of the two aggregate types are not constant. With increasing fraction of sergeants in the mixture, up to approximately 85 mol%, where the fraction of *P*-type aggregates becomes negligible, the fraction of ***R*-Si-BTA** in the

DOI: 10.1021/jacs.7b02835
J. Am. Chem. Soc. 2017, 139, 7036–7044

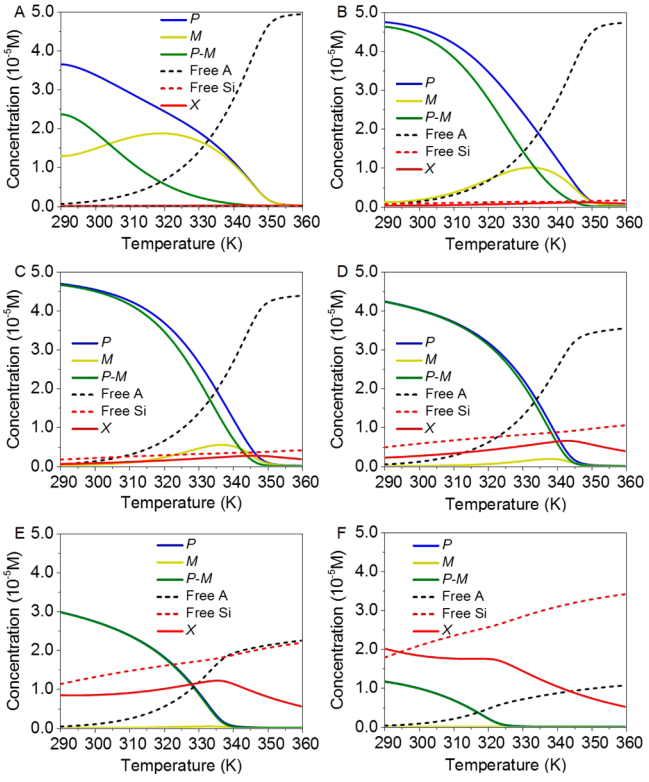

Figure 6. Calculated concentration of BTAs in the various species types (*P*, *M*, and *X*) and concentration of free monomers (A and Si) as a function of the temperature for several fractions of sergeants ***R*-Si-BTA**: 0.5 mol% (A), 4 mol% (B), 10 mol% (C), 25 mol% (D), 50 mol % (E), and 75 mol% (F).

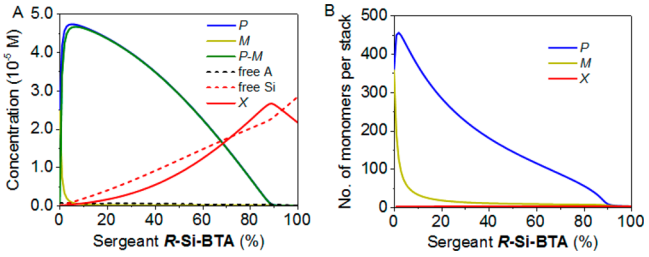

Figure 7. (A) Calculated concentration and (B) average stack length (number of monomers per stack) of the various species types over the fraction of sergeants ***R*-Si-BTA** at 293 K, c_{tot} = 50 μM in MCH.

P-type aggregates increases sub-stoichiometrically, up to a limit of approximately 30 mol%. This analysis suggests that above the fraction of 10 mol% of ***R*-Si-BTA** (where the CD signal is maximum), its propensity to intercalate into *P*-type aggregates becomes lower, which initiates the formation of segregated ***R*-Si-BTA**-dominated *X*-type aggregates in the mixture.

As per the model prediction, we conclude that the drop in the CD intensity with increasing fraction of the sergeants is the outcome of a reduction in both the amount and the average stack length (number of monomers per stack) of cooperative *P*-type aggregates. Since in the "sergeant-and-soldiers" experiment the total monomer concentration remains constant, the amount of **a-BTA** dominated *P*-type aggregates continuously decreases with increasing ***R*-Si-BTA**/**a-BTA** feed ratio thereby causing depletion in the CD signal. By working instead in a solution with increasing fraction of ***R*-Si-BTA** for a fixed concentration of the achiral **a-BTA**, the model with the same thermodynamic parameters predicts a steady rise in the CD signal rather than the drop observed in the "sergeant-and-soldiers" experiment (Figure 8A), due to continuous formation of *X*-type aggregates in the presence of an invariant amount of *P*-type aggregates.

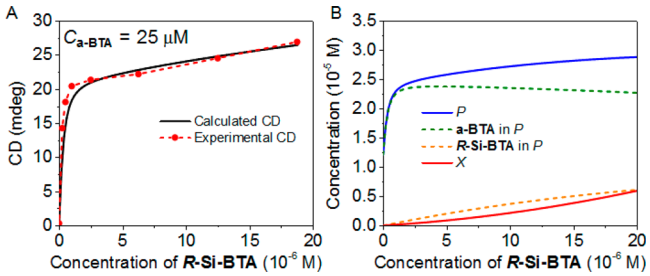

Figure 8. (A) Experimental and calculated CD signal at 220 nm and (B) calculated concentrations of the various species types over increasing fraction of sergeants ***R*-Si-BTA** at a fixed concentration of **a-BTA** 25 μM at 293 K.

To experimentally validate this prediction, we performed a new set of experiments. CD spectra were measured from a set of solutions prepared at fixed $c_{a\text{-}BTA}$ = 25 μM and increasing concentration of ***R*-Si-BTA** (Figure 8A, Figure S9). Indeed an overall rise in the CD signal is observed, with two different slopes in the two regimes that can be rationalized by the model. The first regime, up to 2.5 μM of ***R*-Si-BTA** (i.e., 9 mol% of ***R*-Si-BTA**), exhibits a chiral amplification corresponding to the intercalation of ***R*-Si-BTA** into *P*-type aggregates. In the second part of the titration curve ($c_{R\text{-}Si\text{-}BTA}$ > 2.5 μM), the continuous addition of chiral ***R*-Si-BTA** displays a small enhancement in the CD signal due to limited further intercalation of ***R*-Si-BTA** in *P*-type aggregates as well as the formation of *X*-type aggregates (Figure 8B). Since the contribution of the helical columnar *P*-type aggregates to the CD signal is significantly larger than the contribution of the short *X*-type aggregates, only a small rise is observed in the CD intensity in the second regime compared to the sharp jump in the first regime. The continuous increase in the CD intensity in this experiment rules out the possibility of copolymerization of all the monomers into a single stack type (*X*-type). The formation of only *X*-type aggregates would result in a significant drop in the overall CD signal due to the dominance of ***R*-Si-BTA**, analogous to the drop observed in the "sergeant-and-soldiers" experiment described in Figure 1C. In fact, the presence of two regimes perfectly matches with the coexistence of *P*-type and *X*-type aggregates, as predicted by the model.

DISCUSSION AND CONCLUSIONS

Based on the experimental data and the mathematical model, the entire copolymerization process as studied by the "sergeant-and-soldiers" experiment can be summarized by the cartoon depicted in Scheme 2. Up to nearly 10 mol% of ***R*-Si-BTA**, favorable incorporation of ***R*-Si-BTA** into *P*-type aggregates takes place in a cooperative mechanism, such that the concentration of *P*-type aggregates rapidly increases at the expense of *M*-type aggregates, leading to chiral amplification. Below 10 mol% of ***R*-Si-BTA** in the mixture, the steric hindrance of bulky ***R*-Si-BTA** does not adversely affect its behavior as a sergeant for **a-BTA**, rather ***R*-Si-BTA** prefers to randomly intercalate within predominantly **a-BTA**-based aggregates to minimize its own steric repulsion. However, at 25 mol% of ***R*-Si-BTA** added, the shape of the CD spectra starts

DOI: 10.1021/jacs.7b02835
J. Am. Chem. Soc. 2017, 139, 7036−7044

Scheme 2. Schematic Representation of the Supramolecular Copolymerization Process between a-BTA and *R*-Si-BTA[a]

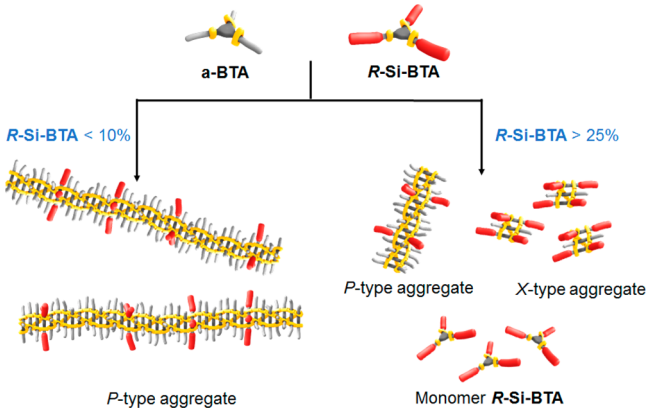

[a]Illustrated are various species types present below 10 mol% and above 25 mol% of ***R*-Si-BTA** added. For clarity, the presence of free **a-BTA** monomers in the system is omitted, as its concentration is very low.

to change indicating a change in the packing within the aggregate. Most likely, the incompatibility between the alkyl and the oDMSi side chains in combination with the isodesmic assembly of the increasing amounts of ***R*-Si-BTA** overrules the favorable steric parameter for copolymerization. This plausibly results in the formation of segregated ***R*-Si-BTA** dominated short *X*-type aggregates, in the presence of *P*-type aggregates in the mixture. With increasing ***R*-Si-BTA/a-BTA** feed ratios, the amount of **a-BTA** dominated *P*-type aggregates continuously drops in the mixture leading to a consistent fall in the CD signal observed in the second regime. Additionally, due to the coexistence of a significant population of the free ***R*-Si-BTA** monomer in the mixtures (Figure 7A), the compositions of the *P*- and *X*-type aggregates change continuously with added ***R*-Si-BTA**.

In conclusion, we reported supramolecular copolymerization under thermodynamic equilibrium conditions between two BTA monomers that bear structurally different alkyl and oDMSi side chains and are distinguished by distinct self-assembly mechanisms. Their co-assembly behavior was analyzed by "sergeant-and-soldiers" CD experiments and in-depth theoretical modeling. A remarkable chiral induction was observed by mixing of two individually CD silent diluted solutions resulting from supramolecular copolymerization between two monomers stacking via cooperative and isodesmic mechanisms. The two regimes observed in the variation of the CD signal of the mixtures were related to the combined effect of sterically demanding self-assembly of ***R*-Si-BTA**, the oDMSi side chain's incompatibility with **a-BTA**, and the difference in mechanism of the homopolymerization of the individual monomers. Below 10 mol% of ***R*-Si-BTA**, the huge chiral amplification originates from the favorable cooperative copolymerization of **a-BTA** soldiers with chiral ***R*-Si-BTA** sergeant into *P*-type aggregates, in which the ***R*-Si-BTA** sergeants completely copolymerize with **a-BTA** to minimize their own steric hindrance. Beyond 25 mol%, the effect gradually diminishes due to both side-chain incompatibility and isodesmic assembly of the dominant bulky ***R*-Si-BTA** monomer, resulting in the segregated formation of ***R*-Si-BTA** dominated *X*-type aggregates along with *P*-type aggregates. As the amount of **a-BTA** monomers and thereby *P*-type aggregates continuously decreases with increasing ***R*-Si-BTA/a-BTA** feed ratios, we observe a continuous drop in the CD signal that predominantly arises from the helical columnar *P*-type aggregate, explaining the biphasic behavior.

An excellent agreement between the experimental results and the model allowed us to quantify the thermodynamic parameters, the concentrations, and the compositions of different aggregates present in the mixtures as a function of various monomer compositions and temperatures during the copolymerization. This example is an illustration of how subtle balances between several parameters such as different monomer compatibilities, relative monomer reactivities, and individual mechanism of homopolymerization are more critical in the construction of supramolecular copolymers than established for covalent copolymerization. The present work is another step toward developing the understanding on the largely unknown area of multicomponent supramolecular copolymerizations in the context of the mechanistic elucidation, thermodynamic stability, and monomer feed-dependent copolymerization behavior. We propose that such a generalized understanding combining spectroscopic studies with explicit theoretical modeling on the complexity of supramolecular copolymerization will pave the way for constructing more complex functional supramolecular materials for future applications.

■ ASSOCIATED CONTENT

Supporting Information

The Supporting Information is available free of charge on the ACS Publications website at DOI: 10.1021/jacs.7b02835.

Additional CD, UV, and IR spectra of ***R*-Si-BTA** and **a-BTA**; fits of the temperature-dependent cooling curves from CD data of homopolymerization; speciation plots of homopolymerization and copolymerization; and description of the equilibrium two-component model (PDF)

■ AUTHOR INFORMATION

Corresponding Authors

*h.m.m.t.eikelder@tue.nl
*a.palmans@tue.nl
*e.w.meijer@tue.nl

ORCID

Albert J. Markvoort: 0000-0001-6025-9557
Anja R. A. Palmans: 0000-0002-7201-1548
E. W. Meijer: 0000-0003-4126-7492

Author Contributions

⊥A.D. and G.V. contributed equally to the work.

Notes

The authors declare no competing financial interest.

■ ACKNOWLEDGMENTS

This work was financially supported by The Netherlands Organization for Scientific Research (NWO-TOP PUNT Grant 10018944) and the Dutch Ministry of Education, Culture and Science (Gravity Program 024.001.035).

■ REFERENCES

(1) (a) Matyjaszewski, K. *Science* **2011**, *333*, 1104−1105. (b) Badi, N.; Lutz, J.-F. *Chem. Soc. Rev.* **2009**, *38*, 3383−3390. (c) Lutz, J.-F.; Ouchi, M.; Liu, D. R.; Sawamoto, M. *Science* **2013**, *341*, 6146. (d) Lutz, J.-F.; Lehn, J.-M.; Meijer, E. W.; Matyjaszewski, K. *Nat. Rev.*

DOI: 10.1021/jacs.7b02835
J. Am. Chem. Soc. 2017, 139, 7036−7044

Mater. **2016**, *1*, 16024. (e) Robertson, E. J.; Battigelli, A.; Proulx, C.; Mannige, R. V.; Haxton, T. K.; Yun, L.; Whitelam, S.; Zuckermann, R. N. *Acc. Chem. Res.* **2016**, *49*, 379−389.

(2) Odian, G. *Principles of Polymerization*, 4th ed.; Wiley: Weinheim, 2004.

(3) (a) Hawker, C. *Acc. Chem. Res.* **1997**, *30*, 373−382. (b) Braunecker, W. A.; Matyjaszewski, K. *Prog. Polym. Sci.* **2007**, *32*, 93−146. (c) Bielawski, C. W.; Grubbs, R. H. *Prog. Polym. Sci.* **2007**, *32*, 1−29. (d) Bates, F. S.; Hillmyer, M. A.; Lodge, T. P.; Bates, C. M.; Delaney, K. T.; Fredrickson, G. H. *Science* **2012**, *336*, 434−440. (e) Ogura, Y.; Terashima, T.; Sawamoto, M. *ACS Macro Lett.* **2013**, *2*, 985−989. (f) Lavilla, C.; Byrne, M.; Heise, A. *Macromolecules* **2016**, *49*, 2942−2947. (g) Gutekunst, W. R.; Hawker, C. J. *J. Am. Chem. Soc.* **2015**, *137*, 8038−8041. (h) Martens, S.; Van den Begin, J.; Madder, A.; Du Prez, F. E.; Espeel, P. *J. Am. Chem. Soc.* **2016**, *138*, 14182−14185.

(4) (a) Brunsveld, L.; Folmer, B. J. B.; Meijer, E. W.; Sijbesma, R. P. *Chem. Rev.* **2001**, *101*, 4071−4097. (b) de Greef, T. F. A.; Meijer, E. W. *Nature* **2008**, *453*, 171−173. (c) De Greef, T. F. A.; Smulders, M. M. J.; Wolffs, M.; Schenning, A. P. H. J.; Sijbesma, R. P.; Meijer, E. W. *Chem. Rev.* **2009**, *109*, 5687−5754. (d) Yang, L.; Tan, X.; Wang, Z.; Zhang, X. *Chem. Rev.* **2015**, *115*, 7196−7239. (e) Krieg, E.; Bastings, M. M. C.; Besenius, P.; Rybtchinski, B. *Chem. Rev.* **2016**, *116*, 2414−2477. (f) Besenius, P. *J. Polym. Sci., Part A: Polym. Chem.* **2017**, *55*, 34−78.

(5) (a) Lehn, J.-M. *Angew. Chem., Int. Ed.* **2015**, *54*, 3276−3289. (b) Aida, T.; Meijer, E. W.; Stupp, S. I. *Science* **2012**, *335*, 813−817. (c) Yan, X.; Wang, F.; Zheng, B.; Huang, F. *Chem. Soc. Rev.* **2012**, *41*, 6042−6065. (d) Liu, K.; Kang, Y.; Wang, Z.; Zhang, X. *Adv. Mater.* **2013**, *25*, 5530−5548. (e) Voorhaar, L.; Hoogenboom, R. *Chem. Soc. Rev.* **2016**, *45*, 4013−4031.

(6) (a) van Nostrum, C. F.; Nolte, R. J. M. *Chem. Commun.* **1996**, 2385−2392. (b) Percec, V.; Glodde, M.; Bera, T. K.; Miura, Y.; Shiyanovskaya, I.; Singer, K. D.; Balagurusamy, V. S. K.; Heiney, P. A.; Schnell, I.; Rapp, A.; Spiess, H.-W.; Hudson, S. D.; Duan, H. *Nature* **2002**, *417*, 384−387. (c) Grimsdale, A. C.; Müllen, K. *Angew. Chem., Int. Ed.* **2005**, *44*, 5592−5629. (d) Kim, F. S.; Ren, G.; Jenekhe, S. A. *Chem. Mater.* **2011**, *23*, 682−732. (e) Moulin, E.; Cid, J.-J.; Giuseppone, N. *Adv. Mater.* **2013**, *25*, 477−487. (f) Babu, S. S.; Prasanthkumar, S.; Ajayaghosh, A. *Angew. Chem., Int. Ed.* **2012**, *51*, 1766−1776.

(7) (a) Cui, H.; Webber, M. J.; Stupp, S. I. *Biopolymers* **2010**, *94*, 1−18. (b) Adler-Abramovich, L.; Gazit, E. *Chem. Soc. Rev.* **2014**, *43*, 6881−6893. (c) Bakker, M. H.; Lee, C. C.; Meijer, E. W.; Dankers, P. Y. W.; Albertazzi, L. *ACS Nano* **2016**, *10*, 1845−1852.

(8) See, for example: (a) Gabriel, G. J.; Iverson, B. L. *J. Am. Chem. Soc.* **2002**, *124*, 15174−15175. (b) Ghosh, S.; Ramakrishnan, S. *Angew. Chem., Int. Ed.* **2005**, *44*, 5441−5447. (c) Wang, C.; Guo, Y.; Wang, Y.; Xu, H.; Wang, R.; Zhang, X. *Angew. Chem., Int. Ed.* **2009**, *48*, 8962−8965. (d) Das, A.; Ghosh, S. *Angew. Chem., Int. Ed.* **2014**, *53*, 2038−2054. (e) Blackburn, A. K.; Sue, A. C. H.; Shveyd, A. K.; Cao, D.; Tayi, A.; Narayanan, A.; Rolczynski, B. S.; Szarko, J. M.; Bozdemir, O. A.; Wakabayashi, R.; Lehrman, J. A.; Kahr, B.; Chen, L. X.; Nassar, M. S.; Stupp, S. I.; Stoddart, J. F. *J. Am. Chem. Soc.* **2014**, *136*, 17224−17235. (f) Chakraborty, S.; Kar, H.; Sikder, A.; Ghosh, S. *Chem. Sci.* **2017**, *8*, 1040−1045.

(9) See, for example: (a) Seto, C. T.; Whitesides, G. M. *J. Am. Chem. Soc.* **1990**, *112*, 6409−6411. (b) Hirschberg, J. H. K. K.; Brunsveld, L.; Ramzi, A.; Vekemans, J. A. J. M.; Sijbesma, R. P.; Meijer, E. W. *Nature* **2000**, *407*, 167−170. (c) Frisch, H.; Unsleber, J. P.; Lüdeker, D.; Peterlechner, M.; Brunklaus, G.; Waller, M.; Besenius, P. *Angew. Chem., Int. Ed.* **2013**, *52*, 10097−10101. (d) Yang, S. K.; Zimmerman, S. C. *Isr. J. Chem.* **2013**, *53*, 511−520. (e) Yang, Z.; Shi, Y.; Chen, W.; Wang, F. *Polym. Chem.* **2015**, *6*, 5540−5544. (f) Ressouche, E.; Pensec, S.; Isare, B.; Jestin, J.; Bouteiller, L. *Langmuir* **2016**, *32*, 11664−11671. (g) Stross, A. E.; Iadevaia, G.; Hunter, C. A. *Chem. Sci.* **2016**, *7*, 94−101.

(10) See, for example: (a) Zhang, G.; Jin, W.; Fukushima, T.; Kosaka, A.; Ishii, N.; Aida, T. *J. Am. Chem. Soc.* **2007**, *129*, 719−722. (b) Babu, S. S.; Praveen, V. K.; Ajayaghosh, A. *Chem. Rev.* **2014**, *114*, 1973−2129. (c) Kumar, M.; Brocorens, P.; Tonnelé, C.; Beljonne, D.; Surin, M.; George, S. J. *Nat. Commun.* **2014**, *5*, 5793. (d) Gorl, D.; Zhang, X.; Stepanenko, V.; Würthner, F. *Nat. Commun.* **2015**, *6*, 7009. (e) van Dijken, D. J.; Stacko, P.; Stuart, M. C. A.; Browne, W. R.; Feringa, B. L. *Chem. Sci.* **2017**, *8*, 1783−1789.

(11) See, for example: (a) Fyfe, M. C. T.; Stoddart, J. F. *Coord. Chem. Rev.* **1999**, *183*, 139−155. (b) Crespo-Biel, O.; Dordi, B.; Reinhoudt, D. N.; Huskens, J. *J. Am. Chem. Soc.* **2005**, *127*, 7594−7600. (c) Leggio, C.; Anselmi, M.; Di Nola, A.; Galantini, L.; Jover, A.; Meijide, F.; Viorel Pavel, N.; Tellini, V. H. S.; Tato, V. J. *Macromolecules* **2007**, *40*, 5899−5906. (d) Zheng, Y.-R.; Zhao, Z.; Wang, M.; Ghosh, K.; Pollock, J. B.; Cook, T. R.; Stang, P. J. *J. Am. Chem. Soc.* **2010**, *132*, 16873−16882. (e) Qiu, H.; Hudson, Z. M.; Winnik, M. A.; Manners, I. *Science* **2015**, *347*, 1329. (f) Li, X.; Gao, Y.; Boott, C. E.; Hayward, D. W.; Harniman, R.; Whittell, G. R.; Richardson, R. M.; Winnik, M. A.; Manners, I. *J. Am. Chem. Soc.* **2016**, *138*, 4087−4095. (g) Lunn, D. J.; Gould, O. E. C.; Whittell, G. R.; Armstrong, D. P.; Mineart, K. P.; Winnik, M. A.; Spontak, R. J.; Pringle, P. G.; Manners, I. *Nat. Commun.* **2016**, *7*, 12371. (h) Nazemi, A.; Boott, C. E.; Lunn, D. J.; Gwyther, J.; Hayward, D. W.; Richardson, R. M.; Winnik, M. A.; Manners, I. *J. Am. Chem. Soc.* **2016**, *138*, 4484−4493.

(12) (a) Wu, A.; Isaacs, L. *J. Am. Chem. Soc.* **2003**, *125*, 4831−4835. (b) Huang, Z.; Yang, L.; Liu, Y.; Wang, Z.; Scherman, O. A.; Zhang, X. *Angew. Chem., Int. Ed.* **2014**, *53*, 5351−5355. (c) Das, A.; Molla, M. R.; Maity, B.; Koley, D.; Ghosh, S. *Chem. - Eur. J.* **2012**, *18*, 9849−9859. (d) Sugiyasu, K.; Kawano, S.-I.; Fujita, N.; Shinkai, S. *Chem. Mater.* **2008**, *20*, 2863−2865. (e) Morris, K. L.; Chen, L.; Raeburn, J.; Sellick, O. R.; Cotanda, P.; Paul, A.; Griffiths, P. C.; King, S. M.; O'Reilly, R. K.; Serpell, L. C.; Adams, D. J. *Nat. Commun.* **2013**, *4*, 1480. (f) Singh, N.; Zhang, K.; Angulo-Pachón, C. A.; Mendes, E.; van Esch, J. H.; Escuder, B. *Chem. Sci.* **2016**, *7*, 5568−5572. (g) Molla, M. R.; Das, A.; Ghosh, S. *Chem. - Eur. J.* **2010**, *16*, 10084−10093. (h) Das, A.; Ghosh, S. *Chem. Commun.* **2011**, *47*, 8922−8924.

(13) Pathway complexity and living supramolecular polymerization: (a) Jonkheijm, P.; van der Schoot, P.; Schenning, A. P. H. J.; Meijer, E. W. *Science* **2006**, *313*, 80−83. (b) Korevaar, P. A.; de Greef, T. F. A.; Meijer, E. W. *Chem. Mater.* **2014**, *26*, 576−586. (c) Ogi, S.; Sugiyasu, K.; Manna, S.; Samitsu, S.; Takeuchi, M. *Nat. Chem.* **2014**, *6*, 188−195. (d) Würthner, F. *Nat. Chem.* **2014**, *6*, 171−173. (e) Kang, J.; Miyajima, D.; Mori, T.; Inoue, Y.; Itoh, Y.; Aida, T. *Science* **2015**, *347*, 646−651. (f) Zhang, W.; Jin, W.; Fukushima, T.; Mori, T.; Aida, T. *J. Am. Chem. Soc.* **2015**, *137*, 13792−13795. (g) Ogi, S.; Stepanenko, V.; Sugiyasu, K.; Takeuchi, M.; Würthner, F. *J. Am. Chem. Soc.* **2015**, *137*, 3300−3307. (h) van der Zwaag, D.; Pieters, P. A.; Korevaar, P. A.; Markvoort, A. J.; Spiering, J. H.; de Greef, T. F. A.; Meijer, E. W. *J. Am. Chem. Soc.* **2015**, *137*, 12677−12688. (i) Mukhopadhyay, R. D.; Ajayaghosh, A. *Science* **2015**, *349* (6245), 241−242. (j) Haedler, A. T.; Meskers, S. C. J. R.; Zha, R. H.; Kivala, M.; Schmidt, H.-W.; Meijer, E. W. *J. Am. Chem. Soc.* **2016**, *138*, 10539−10545. (k) Korevaar, P. A.; George, S. J.; Markvoort, A. J.; Smulders, M. M. J.; Hilbers, P. A. J.; Schenning, A. P. H. J.; de Greef, T. F. A.; Meijer, E. W. *Nature* **2012**, *481*, 492−496. (l) Fukui, T.; Kawai, S.; Fujinuma, S.; Matsushita, Y.; Yasuda, T.; Sakurai, T.; Seki, S.; Takeuchi, M.; Sugiyasu, K. *Nat. Chem.* **2017**, *9*, 493−499.

(14) Theoretical modeling on supramolecular homopolymerization: (a) Zhao, D.; Moore, J. S. *Org. Biomol. Chem.* **2003**, *1*, 3471−3491. (b) Hamacek, J.; Borkovec, M.; Piguet, C. *Dalton Trans.* **2006**, *35*, 1473−1490. (c) Douglas, J. F.; Dudowicz, J.; Freed, K. F. *J. Chem. Phys.* **2008**, *128*, 224901. (d) ten Eikelder, H. M. M.; Markvoort, A. J.; de Greef, T. F. A.; Hilbers, P. A. J. *J. Phys. Chem. B* **2012**, *116*, 5291−5301. (e) Nakano, Y.; Markvoort, A. J.; Cantekin, S.; Filot, I. A. W.; ten Eikelder, H. M. M.; Meijer, E. W.; Palmans, A. R. A. *J. Am. Chem. Soc.* **2013**, *135*, 16497−16506. (f) Fernandez, G.; Stolte, M.; Stepanenko, V.; Würthner, F. *Chem. - Eur. J.* **2013**, *19*, 206−217. (g) Rest, C.; Kandanelli, R.; Fernandez, G. *Chem. Soc. Rev.* **2015**, *44*, 2543−2572. (h) Gershberg, J.; Fennel, F.; Rehm, T. H.; Lochbrunner, S.; Würthner, F. *Chem. Sci.* **2016**, *7*, 1729−1737.

DOI: 10.1021/jacs.7b02835
J. Am. Chem. Soc. 2017, 139, 7036−7044

(15) Supramolecular copolymerization analyzed by computation: (a) Markvoort, A. J.; ten Eikelder, H. M. M.; Hilbers, P. A. J.; de Greef, T. F. A.; Meijer, E. W. *Nat. Commun.* **2011**, *2*, 509. (b) Cantekin, S.; ten Eikelder, H. M. M.; Markvoort, A. J.; Veld, M. A. J.; Korevaar, P. A.; Green, M. M.; Palmans, A. R. A.; Meijer, E. W. *Angew. Chem., Int. Ed.* **2012**, *51*, 6426−6431. (c) Korevaar, P. A.; Grenier, C.; Markvoort, A. J.; Schenning, A. P. H. J.; de Greef, T. F. A.; Meijer, E. W. *Proc. Natl. Acad. Sci. U. S. A.* **2013**, *110*, 17205−17210.

(16) Cantekin, S.; de Greef, T. F. A.; Palmans, A. R. A. *Chem. Soc. Rev.* **2012**, *41*, 6125−6137.

(17) (a) Smulders, M. M. J.; Schenning, A. P. H. J.; Meijer, E. W. *J. Am. Chem. Soc.* **2008**, *130*, 606−611. (b) Stals, P. J. M.; Smulders, M. M. J.; Martin-Rapun, R.; Palmans, A. R. A.; Meijer, E. W. *Chem. - Eur. J.* **2009**, *15*, 2071−2080. (c) Stals, P. J. M.; Everts, J. C.; de Bruijn, R.; Filot, I. A. W.; Smulders, M. M. J.; Martin-Rapun, R.; Pidko, E. A.; de Greef, T. F. A.; Palmans, A. R. A.; Meijer, E. W. *Chem. - Eur. J.* **2010**, *16*, 810−821. (d) Cantekin, S.; Balkenende, D. W. R.; Smulders, M. M. J.; Palmans, A. R. A.; Meijer, E. W. *Nat. Chem.* **2011**, *3*, 42−46. (e) Nakano, Y.; Hirose, T.; Stals, P. J. M.; Meijer, E. W.; Palmans, A. R. A. *Chem. Sci.* **2012**, *3*, 148−155.

(18) Garcia-Iglesias, M.; de Waal, B. F. M.; de Feijter, I.; Palmans, A. R. A.; Meijer, E. W. *Chem. - Eur. J.* **2015**, *21*, 377−385.

(19) "Sergeant-and-soldiers" experiments have been reported for mixtures of two structurally similar achiral and chiral compounds which differ in the presence of only one stereogenic center in the chiral analogue. Here, we extend the designation to mixing of two compounds with different side chains but similar stacking core. (a) Green, M. M.; Reidy, M. P.; Johnson, R. D.; Darling, G.; O'Leary, D. J.; Willson, G. *J. Am. Chem. Soc.* **1989**, *111*, 6452−6454. (b) Palmans, A. R. A.; Vekemans, J. A. J. M.; Havinga, E. E.; Meijer, E. W. *Angew. Chem., Int. Ed. Engl.* **1997**, *36*, 2648−265. (c) Wilson, A. J.; van Gestel, J.; Sijbesma, R. P.; Meijer, E. W. *Chem. Commun.* **2006**, 4404−4406. (d) Prins, L. J.; Timmerman, P.; Reinhoudt, D. N. *J. Am. Chem. Soc.* **2001**, *123*, 10153−10163.

(20) Cantekin, S.; Nakano, Y.; Everts, J. C.; van der Schoot, P.; Meijer, E. W.; Palmans, A. R. A. *Chem. Commun.* **2012**, *48*, 3803−3805.

(21) (a) Veld, M. A. J.; Haveman, D.; Palmans, A. R. A.; Meijer, E. W. *Soft Matter* **2011**, *7*, 524−531. (b) Desmarchelier, A.; Alvarenga, B. G.; Caumes, X.; Dubreucq, L.; Troufflard, C.; Tessier, M.; Vanthuyne, N.; Idé, J.; Maistriaux, T.; Beljonne, D.; Brocorens, P.; Lazzaroni, R.; Raynal, M.; Bouteiller, L. *Soft Matter* **2016**, *12*, 7824−7838.

(22) Concentrations of *P*-, *M*-, and *X*-type (co)polymers shown in speciation plots are always "equivalent concentrations", i.e., the concentration of all the monomers that constitute the considered polymer type. See SI for more details.

DOI: 10.1021/jacs.7b02835
J. Am. Chem. Soc. 2017, 139, 7036−7044